Investigation on the near-field evolution of industrial plumes from metalworking activities

Ari Setyan, Pascal Flament, Nadine Locoge, Karine Deboudt, Véronique Riffault, Laurent Alleman, Coralie Schoemaecker, Jovanna Arndt, Patrick Augustin, Robert Healy, et al.

▶ **To cite this version:**

Ari Setyan, Pascal Flament, Nadine Locoge, Karine Deboudt, Véronique Riffault, et al.. Investigation on the near-field evolution of industrial plumes from metalworking activities. Science of the Total Environment, 2019, 668, pp.443-456. 10.1016/j.scitotenv.2019.02.399 . hal-02552750

HAL Id: hal-02552750
https://hal.science/hal-02552750v1

Submitted on 22 Oct 2021

HAL is a multi-disciplinary open access archive for the deposit and dissemination of scientific research documents, whether they are published or not. The documents may come from teaching and research institutions in France or abroad, or from public or private research centers.

L'archive ouverte pluridisciplinaire **HAL**, est destinée au dépôt et à la diffusion de documents scientifiques de niveau recherche, publiés ou non, émanant des établissements d'enseignement et de recherche français ou étrangers, des laboratoires publics ou privés.

Distributed under a Creative Commons Attribution - NonCommercial 4.0 International License

Version of Record: https://www.sciencedirect.com/science/article/pii/S0048969719309088
Manuscript_fd154c3124fca59886357d1bae99ca8b

Investigation on the near-field evolution of industrial plumes from metalworking activities

Ari Setyan[1,a,b,*], Pascal Flament[1,*], Nadine Locoge[2], Karine Deboudt[1], Véronique Riffault[2], Laurent Y. Alleman[2], Coralie Schoemaecker[3], Jovanna Arndt[4], Patrick Augustin[1], Robert M. Healy[4,c], John C. Wenger[4], Fabrice Cazier[5], Hervé Delbarre[1], Dorothée Dewaele[5], Pascale Dewalle[3,d], Marc Fourmentin[1], Paul Genevray[5], Cyril Gengembre[1], Thierry Leonardis[2], Hélène Marris[1,e], Saliou Mbengue[2,f]

[1] Laboratoire de Physico-Chimie de l'Atmosphère, Université du Littoral Côte d'Opale, EA 4493-CNRS, 59140 Dunkerque, France

[2] Département Sciences de l'Atmosphère et Génie de l'Environnement - SAGE, IMT Lille Douai, Université de Lille, 59000 Lille, France

[3] Laboratoire de Physico-Chimie des Processus de Combustion et de l'Atmosphère, Unité Mixte de Recherche CNRS-Université Lille1 Sciences et Technologies (UMR 8522), 59655 Villeneuve d'Ascq, France

[4] School of Chemistry and Environmental Research Institute, University College Cork, Cork, Ireland

[5] Centre Commun de Mesures, Université du Littoral Côte d'Opale, 59140 Dunkerque, France

[a] now at: Empa, Swiss Federal Laboratories for Materials Science and Technology, Laboratory for Advanced Analytical Technologies, 8600 Dübendorf, Switzerland

[b] now at: ETH Zürich, Institute of Environmental Engineering, 8093 Zürich, Switzerland

[c] now at: Environmental Monitoring and Reporting Branch, Ontario Ministry of the Environment, Conservation and Parks, Ontario, Canada

[d] now at: Unité de Catalyse et Chimie du Solide, Unité Mixte de Recherche CNRS-Université Lille1 Sciences et Technologies (UMR 8181), 59655 Villeneuve d'Ascq, France

[e] now at: Sotrenor, 62710 Courrières, France

[f] now at: CzechGlobe - Global Change Research Institute, 60300 Brno, Czech Republic

[*]**Correspondence to:** Ari Setyan (ari.setyan@gmail.com)
Pascal Flament (pascal.flament@univ-littoral.fr)

Postal address

Prof. Pascal Flament

Université du Littoral Côte d'Opale

Laboratoire de Physico-Chimie de l'Atmosphère - EA 4493

MREI 2 - 189A Avenue Maurice Schumann

© 2019 published by Elsevier. This manuscript is made available under the CC BY NC user license
https://creativecommons.org/licenses/by-nc/4.0/

59140 Dunkerque

Tel : +33 (0)3 28 23 76 44
Fax : +33 (0)3 28 65 82 44

Abstract

In a context where a significant fraction of the population lives near industrial areas, the main objectives of this study are to provide (a) new data on $PM_{2.5}$ chemical compositions, heavy-metal concentrations and trace gases released by metalworking activities and (b) new information on the near-field evolution (up to about a thousand meters) of such industrial plumes in terms of particle chemical composition and size distribution. For that purpose, a one-month field campaign was performed in an industrial area near the city of Dunkirk (Northern France), combining measurements of atmospheric dynamics and physico-chemical characterization of air masses. Comparisons between several elemental ratios (mainly Mn/Fe), particle size distributions and volatile organic compound (VOC) concentrations at the stacks and at a near-field site suggest that plumes of a ferromanganese alloy plant were quickly mixed with pollutants emitted by other sources (mainly other industries, possibly traffic and sea spray), in particular a neighboring steelworks, before reaching the sampling site. This led to the emergence of secondary particles related to condensation and/or aggregation phenomena inside the plumes. Metalworking emissions were also identified as a source of new particle formation, formed through the emission of gaseous precursors and their fast transformation and condensation, over a timescale of minutes before reaching the near-field site 800 m downwind. Ultrafine particles emitted at the stacks also quickly agglomerated to form larger particles before reaching the near-field site. These results show that, even over short distances, the chemical composition and size distribution of metalworking plumes may evolve rapidly and the characteristics of particles at the boundary of an industrial area (especially in contiguous urban areas) may differ from those emitted directly at the stacks.

Keywords
Fine particles
Volatile organic compounds
Industrial emissions
Plume evolution
Atmospheric dynamics

1 Introduction

Epidemiological studies have demonstrated that exposure to atmospheric pollution has adverse effects on human health, such as cardiovascular (Brook et al., 2004) and pulmonary (Oberdörster, 2000) diseases and cancer (Pope et al., 2011). In particular, particles smaller than 2.5 µm ($PM_{2.5}$) are more dangerous than coarse ones ($PM_{2.5-10}$), because the former can penetrate deeper into the lungs, reach the alveoli and enter the cardiovascular system (Kelly and Fussell, 2011). According to the Clean Air for Europe (CAFE, see Table S1 in the supplementary material for acronyms) program, the average decrease of life expectancy in Europe due to exposure to $PM_{2.5}$ is nine months, but increases to 12-36 months in Benelux and in the north-east area of France (2005). However, many uncertainties still remain on the identity of chemicals in the particle phase, their mixing state (which may lead to synergy in terms of toxicity) and source inventories for fine particles bearing toxic chemicals.

Previous studies have shown that industrial activities release large quantities of both gaseous and particulate matter into the atmosphere. The physico-chemical nature of particles emitted by industry has already been reviewed (Riffault et al., 2015; Sanderson et al., 2014; Taiwo et al., 2014). A high variability of chemical composition and size distribution can be observed depending on the type of industrial processes involved. Nevertheless, tracers of specific industrial activities, such as heavy metals (Dall'Osto et al., 2008; Wong et al., 2006; Yang et al., 2018), the organic-to-elemental carbon ratio (OC/EC) (Chow et al., 2011), diagnostic ratios or concentrations of some specific polycyclic aromatic hydrocarbons (PAHs) (Katsoyiannis et al., 2011; Leoni et al., 2016), secondary inorganic species such as ammonium sulfate, nitrate, and chloride (Setyan et al., 2017; Wu et al., 2018), and the carbon preference index (CPI, defined as the ratio of the sum of odd carbon number of n-alkanes to the sum of even carbon number of n-alkanes) (Fraser et al., 2002; Li et al., 2010) have been

identified as a means by which to provide estimates of the relative contribution of pollutant sources from heavily industrialized regions. Many industrial activities emit a range of PAHs, volatile organic compounds (VOCs) and inorganic gases including NO_x and SO_2. For instance, selected industrial processes in steelworks, such as coke production, iron ore sintering (Ciaparra et al., 2009), and electric arc furnaces (Baraniecka et al., 2010), release large amounts of PAHs. Coke ovens, commonly used in steelworks, also emit significant concentrations of VOCs (Lin et al., 2007).

In this context, our NANO-INDUS project had two main objectives: 1) to produce new data on $PM_{2.5}$, carbonaceous particles, heavy-metal concentrations and trace gases released by metalworking activities; and 2) to provide new information on the chemical composition, mixing state and source identification of industrial atmospheric particulate matter.

In terms of atmospheric processes, NANO-INDUS was motivated by three inter-related questions:

1) How much do the physico-chemical characteristics of atmospheric fine particles at the boundary of a metalworking industrial complex differ from those directly emitted from the stacks?

2) Is there a link between the presence of fine particles at the boundary of this site and gases directly emitted from the stacks?

3) Do fine particles within a metalworking plume have a homogeneous chemical composition as essentially primary particles, or are they produced or evolving by condensation and/or agglomeration, leading to secondary particles with heterogeneous compositions?

To help address these questions, a field campaign was conducted at an industrial site close to the Dunkirk metropolitan area (Grande-Synthe). This region is highly industrialized and the

particle concentrations regularly exceed the World Health Organization annual mean guideline value of 10 µg m^{-3} for $PM_{2.5}$ (World Health Organization, 2006). Of particular interest is the industrial area of Grande-Synthe, which is comprised of various industries (steel industry, metallurgy, smelting works, chemical industry, refineries, food-processing industry, power production, cement works) (DREAL, 2011) located 7 km from downtown Dunkirk. Following the diversity of industrial activities at this location, Grande-Synthe is very similar to many other industrial areas throughout the world, where industrial emissions had also been studied in previous publications, e.g. at Port Talbot (United Kingdom) (Dall'Osto et al., 2008), Taranto (Italy) (Amodio et al., 2014), and Hangzhou in the Yangtze River Delta (China) (Dai et al., 2015). Previous studies have also been performed within the industrial park of Grande-Synthe (Cazier et al., 2016; Crenn et al., 2017; Mbengue et al., 2015). Particulate metal content has been extensively studied, due to the importance of steelworks and metallurgy at Grande-Synthe (Alleman et al., 2010; Arndt et al., 2016; Flament et al., 2008; Hleis et al., 2013; Kfoury et al., 2016; Landkocz et al., 2017; Marris et al., 2012; Marris et al., 2013; Mbengue et al., 2014; Mbengue et al., 2017; Santos et al., 2016). A number of elements or elemental ratios have been used as tracers for specific sources within the industrial area, e.g. Mn or Mn/Fe ratio for emissions from the ferromanganese alloy factory (Marris et al., 2012), Pb and Fe isotopes for steelworks emissions (Flament et al., 2008), V and Ni for petrochemistry (Alleman et al., 2010), Fe, Ca, Al and Mn for selected iron and steel processes such as sintering, blast furnace, steelmaking and desulfurization slag processing (Hleis et al., 2013). A few studies have also focused on the measurement of VOCs in this area. For instance, Badol et al (Badol et al., 2008a; Badol et al., 2008b) identified specific industrial activities as important sources of benzene (metallurgical, steel industries), octane (lubricant storage), pentane (hydrocarbon storage), and propene (hydrocarbon cracking). Roukos et al.

(2009) measured BTEX (benzene, toluene, ethylbenzene, xylene) during two contrasting seasons. In winter, BTEX concentrations were mainly due to local pollution, while in summer, they decreased because of photochemical activity and the influence of continental aged air masses, highlighting the fact that even in anthropogenically-influenced areas, long-range transport can have a significant contribution to the observed concentrations. Finally, Xiang et al. (2012) emphasized the influence of vertical turbulence on the dispersion of VOCs at the local scale.

The aim of the present paper is to give an overview of the measurements performed during the NANO-INDUS project, and to present the main findings of this study. First, we will present results obtained during the intensive field campaign performed at the near-field sampling site, and those obtained during the samplings at the stacks. Then, physico-chemical characteristics of particles measured when the near-field sampling site was impacted by plumes from the Fe-Mn plant will be compared to particles measured during periods from other influences (petrochemistry, urban emissions).

2 Experimental

2.1 Sampling site

All sampling and measurements took place next to the site of a ferromanganese alloy manufacturing facility (Fe-Mn plant), located in the industrial area of Grande-Synthe, ~2 km west of the Dunkirk metropolitan area and ~7 km from the city center (51° 01’ 44” north, 2° 16’ 10” east, 10 m above sea level). Figure 1a shows a map of the area with the sampling site

located centrally within the industrial zone of Grande-Synthe and ~800 m southwest of the emission chimneys in the Fe-Mn plant.

Atmospheric composition at the sampling site can be influenced by a variety of different emission sources, depending on the wind direction. Pollutant sources to the east of the sampling site are mainly industrial in origin due to the presence of a large steelworks (< 1 km), but also urban-influenced due to Fort-Mardyck (3'600 inhabitants, ~2 km from the sampling site) and Dunkirk (93'000 inhabitants, ~7 km from the site). The North Sea is only 1 km to the north and northwest, bringing marine and ship emissions to the site. Approximately 200 m to the north of the site is an outdoor storage area for manganese ores which is a potential source of dust during windy periods. Finally, pollutant sources to the west (petrochemistry, glass production) and southwest (refineries) of the site also mainly originate from industrial activities.

The Fe-Mn plant receives iron-enriched manganese ores by boat, and transforms these ores into a ferromanganese alloy, which is used in steelworks to improve the mechanical properties of steel. Figure 2 shows a schematic drawing of the production process. In the first step, manganese ores are sintered with anthracite and calcite ($CaCO_3$) in an oven. This step involves heating of the sinter, followed by cooling. In the second step, the manganese ore included in the sinter is reduced into metallic Mn in an electric arc furnace, which provides the necessary energy for the redox reaction. The third and last step consists of crushing the alloy to obtain the final product. Particles and gases emitted during these steps are collected in three different chimneys, in which they are treated by filters before their release into the atmosphere. Two of these chimneys are located in the sintering unit, above the firing and the cooling areas, respectively, while the third chimney is in the smelting unit. The sintering unit works 24 hours a day with particles and gases continuously emitted from its two chimneys.

Emissions from the smelting unit, where electrochemical reduction of the manganese ore and casting of the final product takes place, occur about once every six hours.

2.2 Instrumentation

The field campaign took place between May 15 and June 12, 2012. The complete list of instruments deployed during this field campaign is given in Table S2. Local meteorological parameters were measured using a weather station (Davis Instruments, Hayward, CA; model Vantage Pro 2) and a sonic anemometer (METEK GmbH, Elmshorn, Germany; model USA-1). A Doppler sonic detection and ranging (SODAR; Remtech, Vélizy, France; model PA2) instrument was used to determine turbulence and vertical profiles of the wind components. An aerosol light detection and ranging (LIDAR; Raymetrics S.A., Paiania, Greece) instrument was installed near the sampling site (Figure 1b). Every 15 minutes, the LIDAR scanned in four different directions, and the backscattered light was used to determine the particle abundance as a function of the altitude and the distance from the instrument.

A large suite of instruments was set up to characterize the concentration, chemical composition and size distribution of particles with a high time resolution (~5 minutes). These instruments were connected to a common isokinetic particle sampler (Alfaro et al., 2003) operated at 52 m^3 hr^{-1}, 7 m above ground level. The Particle Loss Calculator (von der Weiden et al., 2009) was used to calculate particle loss across the sampler (Figure S1 in the supplementary material). The cut-off size of the sampling line was 2.5 µm ($PM_{2.5}$), assuming an average particle density of 2.5 g cm^{-3} based on the measured chemical composition. This high particle density is due to the fact that the sampling site was impacted by a high fraction of sea salts, metal oxide particles (Fe, Mn, Al), and $CaCO_3$ (see Section 4.1). A high-resolution time-of-flight aerosol mass spectrometer (HR-ToF-AMS; Aerodyne Research Inc.,

Billerica, MA) (Canagaratna et al., 2007; DeCarlo et al., 2006) measured the chemical composition and size distribution of non-refractory submicron particles (NR-PM_1) in the range 50-1000 nm (in vacuum aerodynamic diameter, D_{va}). Since this instrument uses a thermal method to vaporize aerosol species, refractory materials, such as black carbon, sea salt and most metallic species, cannot be detected with this technique. An aerosol time-of-flight mass spectrometer (ATOFMS; TSI Instruments Ltd., High Wycombe, U.K.; model 3800-100) (Arndt et al., 2016; Gard et al., 1997) simultaneously measured single particle composition and mixing state in the size range 100-3000 nm (in D_{va}). The ATOFMS vaporizes aerosol species by laser ablation, enabling the measurement of refractory species, which are expected to play a significant role in the particle chemistry at this industrial site. Over 700'000 single particle mass spectra were collected during the campaign and clustered using the K-means algorithm (K=90), as described in detail elsewhere (Gross et al., 2010; Healy et al., 2010; Healy et al., 2009). A 2-wavelength Aethalometer (Magee Scientific, Berkeley, CA; model AE42) was deployed to measure organic-like (OC) and black carbon (BC) concentrations via the measurement of absorption coefficients at 370 and 880 nm, respectively. The algorithm presented by Weingartner et al. (2003) was used to reduce measurement artifacts due to filter loading and the scattering of the light beam in the filter matrix. Two scanning mobility particle sizers (SMPS) and an optical particle counter (OPC) were used to measure the particle size distribution. The first SMPS system (Grimm Aerosol Technik, Ainring, Germany) was comprised of a differential mobility analyzer (DMA; model 55-900) and a condensation particle counter (CPC; model 5.403), enabling particle counting in the size range 10-1000 nm (in mobility diameter, D_m), while the second SMPS (TSI Inc., Shoreview, MN) was constituted of a CPC model 3010, an electrostatic classifier model 3080, and a DMA model 3081, enabling particle counting in the size range 10-480 nm (in D_m). The

OPC (Grimm Aerosol Technik; model 1.108) measured particles in the size range 300 nm - 20 µm (in optical diameter).

In addition to the above-mentioned instruments for online particle measurements, several cascade impactors (Dekati Ltd., Tampere, Finland; 13-stage low pressure impactor, and 3-stage PM_{10} impactors) and a speciation sampler (Thermo Fisher Scientific, Waltham, MA; model Partisol 2300) were also deployed to sample particles on filters for subsequent off-line analyses. These results, some of which have already been published (Mbengue et al., 2014), included the measurement of metals by inductively-coupled plasma mass spectrometry (ICP/MS) (Varian Inc., Santa Clara, CA; model 820-MS; or Perkin Elmer, Waltham, MA; model DRC Elan 6100) and by inductively-coupled plasma atomic emission spectroscopy (ICP/AES) (IRIS Intrepid, Thermo-Scientific), and organic carbon (OC) and elemental carbon (EC) by a thermal-optical method (Sunset Laboratory, Tigard, OR; Lab OC-EC aerosol analyzer).

A proton transfer reaction time-of-flight mass spectrometer (PTR-ToF-MS) (Kore Technology Ltd, Ely, Cambridgeshire, U.K.; model Series I) (de Gouw and Warneke, 2007; Lindinger et al., 1998) allowed for measurement of VOCs with a proton affinity higher than that of water. Long-chain alkanes and aldehydes ($>C_8$) were sampled on adsorbing cartridges with an automatic sampler, and analyzed after thermal desorption by gas chromatography coupled to a mass spectrometer (GC/MS) (Agilent Technologies Inc., Santa Clara, CA; GC: model 6890N; MS: model 5975) following a procedure previously developed and validated (Detournay et al., 2011). Finally, automatic analyzers were used to monitor CO_2 (Horiba Ltd, Kyoto, Japan; model VA-3000) as well as CO (model CO 12M), NO_x (model AC 31M), O_3 (model O_3 41M), and SO_2 (model AF 22M), all from Environnement S.A., Poissy, France.

Sampling at the stacks of the ferromanganese alloy production facility was performed using automatic analyzers for gases (SO_2, CO, NO_x), cascade impactors and adsorbing cartridges for collection of particles and VOCs/PAHs for subsequent off-line analysis (Table S3). PM was collected in the flues of each stack (downstream of the industrial filters) by installing a 3-stage cascade impactor (Dekati Ltd) into the center of the chimney flue. The impactor was equipped with a vertical PM_{10} sampling head and the sampling rate was adapted to the stack flue in order to obtain an isokinetic sample. This sampling meets European standards for stack dust sampling for emission controls. More details can be found elsewhere (Arndt et al., 2016; Mbengue et al., 2014).

Date and time are reported in Coordinated Universal Time (UTC). The local time during this study was Central European Summer Time (CEST), which corresponds to UTC+2:00.

3 Meteorology

3.1 Meteorological conditions and atmospheric dynamics

Figure 3 shows the time series of standard meteorological parameters (temperature, relative humidity, solar radiation, rainfall, wind direction and speed) observed during the measurement period, along with atmospheric stability, while back trajectory analysis is presented and discussed in the supplementary material (Figures S2-S4). The temperature varied between 6 and 24°C, but for most of the field campaign, was in the range 10-15°C. The maximum solar radiations were in the range 750-850 W m^{-2}. Several occasional rainy periods occurred during the field campaign, especially after June 2. The relative humidity was rather high (mean ± 1 σ: 78.9 ± 14.3%) due to the coastal location of the receptor site.

The wind direction was an important parameter to identify periods during which the site was under the influence of metalworking emissions, and in particular when NE winds could transport plumes from the emission stacks of the Fe-Mn plant to the sampling site. The wind direction was variable during the field campaign, as shown by the wind rose plot (Figure 1c). Three dominant wind directions each with an occurrence rate of 15-20% were observed, corresponding to winds blowing from the southwest, northwest, and north. The wind was northeasterly for about 5% of the field campaign, and we identified two periods during which the plume could be transported to the site from this direction: May 25-27, and June 2. The period between May 25 and 27 was the longest period with a NE wind, corresponding to the hottest days of the campaign and elevated solar irradiation (~800 W m^{-2}), which could increase photo-oxidation and promote relatively faster chemical transformations of particles and precursor gases between the emission stacks and the sampling site. Moreover, a high temperature gradient also promotes sea breezes, and thus a vertical mixing of the plumes (see below).

During these NE wind periods, it is important to assess the stability of the atmosphere, which describes the mixing of emissions over a large area and explain the vertical and horizontal dispersion of the plume. In the current study, the Monin-Obukhov length scale (deduced from the sonic anemometer), which depends mainly on heat and momentum fluxes, friction velocity and temperature, has been used to estimate the atmospheric stability classes (Stull, 1988). Figure 3d shows the time series of the atmospheric stability during the whole campaign. High occurrences of unstable periods were observed and represent ~47% and 17% of unstable and very unstable atmospheric conditions, respectively, thus favoring plume dispersion. Moreover, LIDAR measurements can confirm this dispersion effect, and that plumes effectively reach the sampling site during NE wind periods (see below).

306 Winds were blowing from NW to NE on 18 days during the campaign, while 11 sea breeze
307 events were also observed. Sea breezes have been frequently observed at Dunkirk during
308 previous studies (Boyouk et al., 2011; Roukos et al., 2011; Talbot et al., 2007). Sea breeze
309 coming from the sea toward the land may modify the lower troposphere stratification by the
310 formation of a thermal internal boundary layer (TIBL) (Augustin et al., 2006). The TIBL is a
311 thin unstable layer where pollutants can be trapped and mixed. Furthermore, since the
312 SODAR echo depends on fluctuation of temperature due to the signature of the boundary
313 layer top, the TIBL top, characterized by high echo values, can be detected (Beyrich, 1997).
314 During the present campaign, the NE wind period between May 25 and May 27 is of
315 particular interest, because according to the wind direction and wind speed time-height
316 sections from the SODAR (Figure 4a), these three days are characterized by long sea breeze
317 events (e.g. on May 25 from 10:00 am to 8:00 pm, on May 26 from 9:00 am to 8:00 pm, and
318 on May 27 from 11:00 am to 8:00 pm), with winds at ground level coming mainly from the
319 NE and likely transporting plumes from the Fe-Mn plant to the sampling site. According to
320 Figure 4e, these sea breeze events are also characterized by an increase in the concentration of
321 particulate phase organics and ammonium nitrate, and a decrease in the concentration of
322 sulfate. These results suggest that organics and ammonium nitrate could possibly be emitted
323 by metalworking activities.

324 **3.2 Detection and monitoring of metalworking plumes**

325 Ground-based remote sensing instruments (SODAR and LIDAR) were used to monitor the
326 propagation of metalworking plumes in the vicinity of the sampling site. Figure 4 includes the
327 SODAR, LIDAR, AMS, Aethalometer, and SMPS data during the period 25-27 May when
328 the winds were from the NE and sea breezes were observed, while Figure S5 shows a few

examples of LIDAR vertical scans for four relevant directions. The LIDAR data shown in Figures 4b and S5 correspond to the depolarization ratio at 355 nm, i.e. the ratio between the measured perpendicular and parallel backscattered LIDAR signals. This parameter provides information in order to distinguish spherical (e.g. haze) from non-spherical particles (e.g. dust and smoke) in the atmosphere. For example, non-spherical particles as industrial dust (e.g. fly ash from metalworking or steelworks) can depolarize LIDAR signals, resulting in high depolarization ratio values. The higher 355 nm-depolarization ratios were observed during 25-27 May sea breeze events (Figure 4b), clearly indicating that during these precise time slots our sampling site was influenced by metalworking plumes.

To confirm the identification of periods during which the sampling site was specifically impacted by these plumes, a two-steps analysis of SODAR and LIDAR data was performed. First, the SODAR data (Figure 4a) was used to determine periods during which the wind at ground level was coming from the NE. Then, the LIDAR data for these periods (Figures 4b and S5) was used to determine whether the sampling site was under the influence of the plumes, as well as to confirm the origin of these plumes. For instance, Figure S5d shows a LIDAR vertical scan measured toward an azimuth angle of 228°, corresponding to the direction of the sampling site (Figure S5e). This scan shows that a plume was located very close to the sampling site. LIDAR scans measured less than an hour earlier toward the stacks (azimuth angle 13°, Figure S5a) and the azimuth angles 308° (Figure S5b) and 238° (Figure S5c) helped us to determine that the plume was mainly coming from the stacks of the Fe-Mn plant, possibly mixed with emissions from the nearby steelworks.

4 Results and discussion

4.1 Particle chemical composition

Figure 5b shows the time series of the five NR-PM_1 species measured by the HR-ToF-AMS, along with BC measurements from the Aethalometer. The average NR-PM_1 concentration during the study was 10.7 µg m^{-3}. This mean value, taking only NR-PM_1 into account, slightly exceeds the WHO recommendations (10 µg m^{-3}). Concentrations were very high between May 24 and May 27 (in the range 20-75 µg m^{-3}), but decreased significantly after June 5 (below 5 µg m^{-3}). According to meteorological conditions and atmospheric dynamics during these periods (Section 3), high mass loadings were concurrent with low wind speed coming from the northeast and east (metalworking activities sector), while the decrease in particle mass loading during the last week occurred when the wind speed increased significantly and wind direction shifted to the south, bringing a few rain episodes. NR-PM_1 was dominated by inorganic species, which accounted for ~2/3 of the total mass, while organics accounted for ~1/3 (Figure 5, upper pie chart). However, the chemical composition varied significantly throughout the study, and several pollution events dominated by ammonium nitrate, ammonium sulfate or organics were observed, especially downwind of metalworking emissions. Despite the fact that very few studies emphasized the contribution of non-refractory submicron aerosols (NR-PM_1) to metalworking (steel industry, metallurgy, smelting works) emissions (Almeida et al., 2015; Crenn et al., 2017), this confirms the importance of secondary aerosols in these emissions. We also observed several periods with an increase in the non-refractory chloride concentration up to ~5 µg m^{-3}. This chloride does not correspond to sea salt, given that the AMS, operated in standard conditions (with the vaporizer set at 600°C), cannot evaporate and measure NaCl. Examination of the dependence

of chloride mass concentrations upon wind direction indicates that this species was observed only during NE wind periods, i.e. when the sampling site was under the direct influence of the Fe-Mn plant and the adjacent steelworks. Moreover, chloride was found to be very well correlated with the K^+ fragment of the AMS (r^2=0.67), suggesting that chloride was mainly present in the form of KCl. This might be due to the high formation of KCl during the sintering process in steelworks (Hleis et al., 2013; Ji et al., 2017; Peng et al., 2009) and is consistent with previous observations using the same instrument at a nearby location (Crenn et al., 2017). Thus, the non-refractory chloride signal may be a useful proxy to determine periods during which a receptor site is under the influence of emissions from steelworks.

This is confirmed by complementary data obtained using the ATOFMS (Figure 5c), which identified 34 distinct particle classes that were subsequently grouped into 10 general categories for clarity. Sea salt particles dominated the dataset by number (24.4% of total spectra), followed by K-containing particles (23.2%) and EC (23.1%). The remaining particle classes correspond to Fe-containing (5.0%), Ca-containing (1.7%), OC and PAH-containing (1.7%), V-containing (1.4%), Mn-containing (1.2%), Pb-containing (1.1%), and other metals (17.1%, including Zn and, in addition, S- and amine-containing particles). Most particle classes are associated with industrial sources (Arndt et al., 2016), based on their composition and wind dependence. K-containing particles are usually associated with biomass burning sources, especially in winter in this region, however domestic wood burning is expected to be negligible at this time of year (May/June). The significant abundance of K-containing particles is consistent with the high signal for non-refractory chloride observed by the AMS and confirms the importance of steelworks sintering emissions containing KCl. EC particle numbers increased towards the end of the sampling period, while OC and PAH-containing particles were detected in their largest numbers on June 2. EC-containing particles were more

plentiful during E-NE wind periods (Figure 5a-c), i.e. when the sampling site was more specifically under the influence of the nearby coke production facility of the integrated steelmaking plant. Weitkamp et al. (2005) showed that elemental carbon contributes up to 30 wt.% to coke production emissions. Ca-containing, Fe-containing and Mn-containing particles clearly increase on May 25, 26 and 27 (downwind of the metalworking emissions), while the latter two categories (Fe- and Mn-containing particles) also increased sharply on May 17, under the influence of urban emissions. Given their composition and size, particles in these categories are almost certainly emitted by either the ferromanganese alloy production plant or the neighboring steelworks. This is supported by the fact that these particles are detected in higher numbers during periods when meteorological conditions were most favorable for plumes to be transported from these two plants, as monitored by LIDAR sensing (see Section 3.2). Further discussion and interpretation of the ATOFMS data, including the other metals category, will be the subject of future publications.

Figure 6 represents the time series of size-resolved elemental composition, determined by ICP/MS and ICP/AES analysis of filters collected using a 13-stage impactor with a time resolution of 24 or 48 hours, while Figure 7a shows the time series of the mass concentration. The concentration of the following elements increased significantly during the periods May 25-27 and June 1-3, when the wind was predominantly coming from the metallurgical complex (NE winds): Fe, Mn, Ca, K, Zn, Pb, plus a few minor elements (Cu, Ti, Ba, Rb, Sr). The size distribution indicates that some elements are enriched in the submicron fractions, (K, Zn, Pb, V, Ni, Cr, Rb, Mo, As, Cd, Sb), while others are more abundant in the coarse fraction (Fe, Ca, Mn, Ti, Ba, Sr), depending on the wind direction. The fact that both Mn and Fe, abundant downwind of ferromanganese- and steelworks-emissions, were more concentrated in the coarse fraction may be due to a combination of (i) the resuspension of dust from the

422 iron-enriched manganese ores stored outdoors (Figure 1b), (ii) industrial mechanical
423 processes (excavating, crushing or ore pile processing), in addition to stationary emissions
424 (sintering, etc.), and (iii) road dust resuspension in the harbor area. The comparison between
425 elemental ratios at the emission stacks of the Fe-Mn alloy plant and at the sampling site has
426 been used to confirm periods during which the sampling site was under the influence of
427 emissions from this plant (Table 1). Among the three plant stacks, the one located above the
428 cooling area of the sintering unit (stack B, Figure 2) was by far the most important emitter of
429 fine particles (Arndt et al., 2016), ~4 times more than stack A (firing area) and ~50 times
430 more than stack C (smelting unit) (Figure 7b). Given that the plant was manufacturing
431 ferromanganese alloy, the most suitable proxy for our analysis is the Mn/Fe ratio (Marris et
432 al., 2012). Emissions from the stacks of the plant show an enrichment of Mn compared to Fe,
433 with a Mn/Fe ratio around 3 (Table 1). At the near-field site, the Mn/Fe ratio remained below
434 1, except for two periods (May 19-21 and May 31-June 1) when both metal concentrations
435 were very low. In addition, the Mn/Fe ratio during the two periods under the influence of NE
436 winds (May 25-27 and June 1-3) was in the range 0.3-0.4. This result, coupled with the
437 increase of potassium from KCl (steelworks sintering emissions proxy) observed by the HR-
438 ToF-AMS during the same periods, suggests that the plumes emitted by the Fe-Mn plant were
439 mixed, before reaching the sampling site, with emissions from the adjacent steelworks, for
440 which the Mn/Fe ratio is very low (<0.01) (Alleman et al., 2010). Other elemental ratios
441 reported in Table 1 show that values calculated for the near-field site are very different from
442 those determined at the stacks, suggesting that the plumes were quickly (within a few
443 minutes) mixed with pollutants emitted by other sources (e.g. steelworks, truck traffic in the
444 industrial zone) (Mbengue et al., 2017) before reaching the sampling site. This is certainly
445 due to the unstable atmospheric conditions prevailed most of the time during the sampling

campaign (Figure 3d), favoring plumes dispersion. This is especially true during sea breeze events, with the formation of an unstable TIBL, as those unambiguously identified during the May 25-27 period, the longer sea breeze episode of the field campaign.

4.2 Particle size distributions

Figure 8 shows the time series of the particle number size distribution between 10 and 500 nm, along with the average size distribution for the entire study. The average size distribution has a single mode at 40 nm (in D_m). However, the particle number concentrations and size distributions varied dynamically during the study. Several periods displayed an increase in the particle number concentration. During most of these periods, size distributions were unimodal with a mode centered at 40-60 nm (e.g. May 19, 28, 29, 30, June 1). However, size distributions observed during NE wind periods (May 25-27, June 2) were very different, and showed a mode at much smaller sizes, below 20 nm. This observation was also quite obvious during sea breeze events on May 25-27 (Figure 4d), systematically associated with an increase in particles of small sizes centered at around 20 nm. The presence of this nucleation mode when the sampling site was under the direct influence of metalworking emissions suggests the occurrence of new particle formation events. New particle formation is a phenomenon which has been extensively observed at various urban, remote, and coastal locations (Curtius, 2006; Holmes, 2007; Kulmala et al., 2004; Zhang et al., 2012). Thus, these events may occur in polluted as well as in very clean environments. Usually, when new particle formation and growth events occur at a regional scale, the SMPS data trend line shows a “banana shape”. Indeed, an increase of the concentration of very small particles (<15 nm) is first observed when these new particles are formed. Then, an increase of the mode is observed during the following hours, when gaseous compounds with low volatility condense

onto the surface of these new particles, or when these particles agglomerate to form bigger ones (Setyan et al., 2014; Setyan et al., 2012). The absence of "banana shapes" and the presence of a constant nucleation mode during several hours in the present SMPS dataset (Figure 4d) suggest that new particle formation was due to continuous emissions from a single point source, located at a constant distance from the near-field sampling site. This may be due to major emissions of these new particles or gaseous precursors from the Fe-Mn plant stacks (or adjacent steelworks emissions), which undergo rapid cooling in the ambient air, thus promoting fast condensation of the gaseous emissions and transformation of stack pipe generated particles, before reaching the sampling site.

Another evidence for new particles formation and growth is emphasized by mass size distribution measurements. Figure 7a shows the mass size distributions determined at the sampling site with the 13-stage impactor. $PM_{2.5}$ concentrations varied in the range of 11-44 µg m^{-3} during this study. The highest concentrations observed during the whole field campaign were reached when the wind was coming from the NE direction at relatively low speed, which counteracted dilution of the plumes. The total mass was dominated by submicron particles (from 0.1 to 1 µm), which accounted for 63.1% of the mass, while particles larger than 1 µm accounted for 33.5%. Particles in the ultrafine size range (<0.1 µm) had a negligible contribution to the mass (3.4%), even if their number was much higher than particles of larger sizes. The mass size distributions did not fluctuate drastically during the study, except for two periods. Between May 15-17, the mass was dominated by coarse particles (65% of the total, with probably a high contribution of sea salts, considering the wind direction and results from ATOFMS and ICP/MS – Figures 5c and 6), while from May 29-31, the contribution of submicron particles was higher (77% of the total mass).

These size distributions observed at the near-field site were very different to those observed at the stacks of the Fe-Mn plant (Figure 7b). Emissions from the plant were totally dominated by particles in the ultrafine range (60.1% of particles <0.1 µm), while these particles accounted for only 3.4% at the near-field site. These observations provide further evidence to support the fast evolution of the plumes and also indicate that emissions from the stacks are likely very quickly diluted in an air mass containing larger particles before reaching the sampling site. In the presence of those larger particles, ultrafine particles freshly emitted at the stacks may quickly agglomerate to form larger particles before reaching the sampling site. In summary, ultrafine particles (D_m ~20 nm) seem to be continuously generated by Fe-Mn plant and steelworks emissions, but within the plumes fast agglomeration processes could result, in a few minutes, in the formation of larger particles in the accumulation mode (0.1-1.0 µm).

4.3 Trace gases

Figure 5f-h shows the time series of several VOC families (aromatics, alkanes, alkenes, oxygenated VOCs, biogenic VOCs). Most of them exhibited high concentrations during the first five days of the campaign (May 15-19), then decreased significantly until the end of the study. However, some short events are also apparent, especially during the NE wind periods, i.e. under the influence of metalworking activities. Benzene was the only VOC to increase significantly when the sampling site was under the influence of emissions from the Fe-Mn plant and steelworks. Toluene also increased during these periods, but to a lesser extent. Toluene and benzene were by far the most concentrated VOCs released from the stacks of the Fe-Mn factory, especially from the stack above the firing area, with a toluene/benzene ratio in the range 2-3. However, during NE wind periods, the toluene/benzene ratio was always ~0.5 at the sampling site, similar to the ratio previously measured in the same area (Roukos et al.,

2009). This result implies either that emissions from the stacks were already highly processed when the plumes reached the sampling site (as evidenced previously for particles), or that there was another important source of benzene near the Fe-Mn plant (e.g. the steelworks, Ciaparra et al., 2009). Several additional events were identified, such as during the nights of May 22-23, May 23-24, and May 31-June 1, with an increase of short-chain alkanes (Figure 5g). These events took place during NW and W wind periods, suggesting that short-chain alkane emissions could possibly be related to petrochemical industrial activities in the area (Figure 1a).

On the bottom right of Figure 5, two pie charts show the average VOC composition during NE wind periods (downwind metalworking sources) and measured at the stacks. VOCs emitted at the stacks are totally dominated by aromatic compounds (mainly toluene and benzene), which account for 60% of the total measured VOCs, while this class of compounds accounts for only 31% at the sampling site during NE wind periods. These pie charts also show that oxygenated compounds emitted at the stacks represent 7% of the total VOCs, while at the sampling site, they account for 27% of the total VOCs. Moreover, none of the oxygenated compounds identified at the sampling site come from aromatic precursors. These results suggest that emissions from the stacks are, during NE wind periods, quickly diluted in an aged air mass before reaching the sampling site. This also confirms previous observations within the same industrial complex (Roukos et al., 2009) that highlighted the fact that even in anthropogenically-influenced areas, long-range transport can have a significant contribution to the observed concentrations of gaseous pollutants.

Figure 5d-e shows the time series of the main trace gases (CO, CO_2, NO_x, O_3, SO_2). Among them, CO_2 and O_3 were the only gases to show significant diurnal trends. O_3 varied between 20 ppb (nighttime) and 40 ppb (daytime) on average. The average CO_2 concentration was 460

539 ppm during the night and 430 ppm during the day. Its diurnal pattern was mainly driven by
540 boundary layer dynamics. Vegetation and variation in the surface temperature of the sea could
541 also influence the diurnal pattern of CO_2. The concentration of the other gases varied
542 dynamically throughout the study. CO and SO_2 increased significantly during NE wind
543 periods, when the sampling site was under the direct influence of metallurgical emissions.
544 The CO concentration during these periods was in the range 3-10 ppm, ~10 times higher than
545 during other periods. The SO_2 concentration also increased 10-fold during NE wind periods.
546 Measurements performed at the stacks of the Fe-Mn factory confirmed that the firing area of
547 the sintering unit of the plant emitted very large amounts of these two gases (Table 2).
548 Sulfuric acid is one species commonly involved in particle nucleation, along with water
549 (Holmes, 2007; Zhang et al., 2012). Therefore, the very high amounts of SO_2 emitted by this
550 factory, followed by its rapid oxidation to sulfuric acid, could play a major role in the new
551 particle formation events observed at the sampling site downwind of metalworking emissions
552 (Section 4.2). However, for the period of sea breezes during which the sampling site was
553 unambiguously influenced by metalworking plumes (Figure 4b and 4d), organics in NR-PM_1
554 are clearly more abundant than sulfates (Figure 4e). Thus, after the formation of new particles,
555 which have a diameter of a few nm, the growth of these particles up to larger sizes could be
556 more driven by organics than by sulfate formation, or results from fast agglomeration
557 processes with preexisting particles.

558 **4.4 Physico-chemical characteristics of plumes influenced by different pollutant**
559 **sources**

560 Considering the atmospheric dynamic from LIDAR and SODAR data (section 3), three short
561 time (30 minutes) but highly specific events were identified, influenced by steelworks and Fe-

562 Mn plant activities (from NE-E wind direction), by petrochemical activity (from NW wind
563 direction) and by urban activities (from SE wind direction), respectively. The corresponding
564 gas and particle parameters are listed in Table 2, while Figure 9 shows the average particle
565 number size distributions during these three thirty-minute periods. The particle ($PM_{2.5}$, sum
566 NR-PM_1 and particles number concentrations) and gas (CO, SO_2) concentrations were very
567 high in the metalworking emissions. Indeed, the total NR-PM_1 concentration in this plume
568 was 37.7 µg m^{-3}, much higher than in the plume from the refinery in the NW (16.2 µg m^{-3})
569 and from the urban traffic in the S (2.9 µg m^{-3}), while the particle number concentration was
570 around 20-30 times higher. In terms of chemical composition, the contributions of nitrate
571 (22.3%, vs. 12.3% for petrochemistry and 13.8% for urban emissions) and non-sea salt
572 chloride (6.9%, vs. 1.2% and 3.4%) were significantly higher, and that of sulfate lower
573 (12.7%, vs. 50.0% and 24.1%) in the plume from the metallurgy plant and steelworks,
574 compared to the two other plumes. Results obtained with the ATOFMS (Table 2) showed that
575 most metal-containing particles were also mainly coming from the metallurgical area, such as
576 Fe- and K-rich particles. In addition to these, Ca, Pb, and other metals-rich particles were also
577 present in much higher concentrations when the near-field site was under the influence of
578 metallurgical emissions. Among the trace gases, CO and SO_2 were significantly higher during
579 the NE-E wind period, compared to other periods, and thus their presence was highly
580 influenced by these industrial activities. The presence of high mixing ratios of SO_2 (47.8 ppb),
581 and low contributions of sulfate during the NE-E wind period suggest that chemical
582 processing was not fast enough to totally oxidize SO_2 to sulfate over a distance of <1 km,
583 even if new particle formation events were observed at the sampling site during this NE-E
584 wind period (see Section 4.3). However, considering metal-bearing particles as a proxy for
585 refractory compounds, the latter contribution to particles smaller than 100 nm is relatively low

586 during NE wind periods (Figure 6, May 23-25 and May 25-27 samples). This size fraction is
587 then probably dominated by the non-refractory fraction, and notably by organic compounds
588 which account for 45 % or NR-PM_1 concentration during the plume from the NE-E (Table 2).
589 This result strongly suggests that after the formation of new particles in the plume from the
590 metallurgical area, their growth to larger sizes was largely driven by the condensation of
591 organics.

592

593 **5 Conclusion**

594 The aim of the NANO-INDUS project was to study the evolution of physico-chemical
595 characteristics of fine particles emitted by industrial activities over a short distance, before
596 they reach surrounding populated areas. This was performed in two steps. First, particles
597 emitted by a ferromanganese alloy plant, located in a multi-influenced industrial area, were
598 directly sampled and analyzed. Secondly, a field campaign was undertaken in the near-field of
599 the plant chimneys, in order to determine the concentration, chemical composition, and size
600 distribution of the fine particles emitted in this multifaceted atmospheric environment.

601 Results obtained during the field campaign showed that unstable atmospheric conditions
602 inside the thermal internal boundary layer (TIBL), due to the occurrence of sea breezes,
603 promote entrapment and mix of pollutants (here Fe-Mn plant emissions, mixed with
604 emissions from an adjacent steelworks). These TIBL unstable periods were characterized by a
605 very high mass concentration of fine particles (38 µg m^{-3} NR-PM_1), compared to other
606 periods dominated by urban or marine influences. These results highlight the huge influence
607 of metalworking emissions on ambient air quality and raise questions about occupational
608 exposure of workers. The chemical composition of particles during these sea breeze periods

was also characteristic, as the contribution of metal-rich particles, organics, and nitrates increased significantly, while that of sulfate decreased, compared to other periods. In addition to new particle formation at the stacks of the Fe-Mn plant, particle growth was also observed in the plume from the metallurgical area. In parallel to possible fast agglomeration processes with preexisting particles, the latter phenomenon was mainly driven by the condensation of organics.

This work has important implications in terms of air quality monitoring strategies. First, people working in an industrial area may be continuously exposed to fine particle concentrations going well beyond recommendations from Public Health Authorities (e.g. the WHO annual mean guideline value of 10 μg m^{-3} for $PM_{2.5}$). Second, our results show that, even over short distances, the chemical composition and size of these fine particles may evolve rapidly, and that their characteristics at the boundary of an industrial complex may differ from those directly emitted at the stacks, the only position monitored by manufacturers to comply with regulation and develop emission control strategies. Generally speaking, it is therefore suggested, for towns increasingly influenced by such activities, that air quality management plans address these observations, for example by means of special monitoring in neighboring urban zones, dedicated to the apportionment of processed metalworking emissions.

Author contribution

PF, NL, KD, VR, LYA, CS, and JCW designed the study. AS, PF, NL, KD, VR, LYA, and CS organized the field campaign at the Fe-Mn plant. AS, PF, NL, KD, VR, LYA, CS, JA, PA, RMH, FC, DD, PD, MF, PG, TL, HM, and SM participated in the data acquisition during the

field campaign and worked on the data treatment. All the co-authors participated in the interpretation of the results. AS wrote the manuscript, with contributions from PA and MF for the sections on atmospheric dynamics and metalworking plume detection. All the co-authors gave their feedback on the different versions of the manuscript, and approved the final version.

Acknowledgements

The NANO-INDUS project was funded by the French Environment and Energy Management Agency (ADEME), grant N° 11-81-C0089. IMT Lille Douai, LPCA and PC2A participate in the CaPPA (funded by the ANR through the PIA) and CLIMIBIO projects, both also funded by the "Hauts-de-France" Regional Council and the European Regional Development Fund. HM and JA acknowledge support from the ADEME and the Irish Research Council, respectively. The authors would also like to thank Emmanuel Fiani (ADEME) for fruitful discussions, François Blond (Glencore Manganèse France) for logistic assistance during the field campaign, and Philippe Le Louer (LECES) for the samplings at the chimneys.

Declarations of interest

None.

References

Commision Of The European Communities. Vol SEC (2005) 1133. Brussels, 2005.

World Health Organization. Air quality guidelines for particulate matter, ozone, nitrogen dioxide and sulfur dioxide - Summary of risk assessment, Geneva (Switzerland), 2006.

Alleman LY, Lamaison L, Perdrix E, Robache A, Galloo J-C. PM10 metal concentrations and source identification using positive matrix factorization and wind sectoring in a French industrial zone. Atmospheric Research 2010; 96: 612-625.

Almeida SM, Lage J, Fernández B, Garcia S, Reis MA, Chaves PC. Chemical characterization of atmospheric particles and source apportionment in the vicinity of a steelmaking industry. Science of The Total Environment 2015; 521-522: 411-420.

Amodio M, de Gennaro G, Di Gilio A, Tutino M. Monitoring of the Deposition of PAHs and Metals Produced by a Steel Plant in Taranto (Italy). Advances in Meteorology 2014; 2014: 10.

Arndt J, Deboudt K, Anderson A, Blondel A, Eliet S, Flament P, et al. Scanning electron microscopy-energy dispersive X-ray spectrometry (SEM-EDX) and aerosol time-of-flight mass spectrometry (ATOFMS) single particle analysis of metallurgy plant emissions. Environmental Pollution 2016; 210: 9-17.

Augustin P, Delbarre H, Lohou F, Campistron B, Puygrenier V, Cachier H, et al. Investigation of local meteorological events and their relationship with ozone and aerosols during an ESCOMPTE photochemical episode. Ann. Geophys. 2006; 24: 2809-2822.

Badol C, Locoge N, Galloo J-C. Using a source-receptor approach to characterise VOC behaviour in a French urban area influenced by industrial emissions: Part II: Source contribution assessment using the Chemical Mass Balance (CMB) model. Science of The Total Environment 2008a; 389: 429-440.

Badol C, Locoge N, Léonardis T, Galloo J-C. Using a source-receptor approach to characterise VOC behaviour in a French urban area influenced by industrial emissions Part I: Study area description, data set acquisition and qualitative data analysis of the data set. Science of The Total Environment 2008b; 389: 441-452.

Baraniecka J, Pyrzyńska K, Szewczyńska M, Pośniak M, Dobrzyńska E. Emission of polycyclic aromatic hydrocarbons from selected processes in steelworks. Journal of Hazardous Materials 2010; 183: 111-115.

Beyrich F. Mixing height estimation from sodar data - A critical discussion. Atmospheric Environment 1997; 31: 3941-3953.

Boyouk N, Léon J-F, Delbarre H, Augustin P, Fourmentin M. Impact of sea breeze on vertical structure of aerosol optical properties in Dunkerque, France. Atmospheric Research 2011; 101: 902-910.

Brook RD, Franklin B, Cascio W, Hong YL, Howard G, Lipsett M, et al. Air pollution and cardiovascular disease - A statement for healthcare professionals from the expert panel on population and prevention science of the American Heart Association. Circulation 2004; 109: 2655-2671.

Canagaratna MR, Jayne JT, Jimenez JL, Allan JD, Alfarra MR, Zhang Q, et al. Chemical and microphysical characterization of ambient aerosols with the Aerodyne aerosol mass spectrometer. Mass Spectrometry Reviews 2007; 26: 185-222.

Cazier F, Genevray P, Dewaele D, Nouali H, Verdin A, Ledoux F, et al. Characterisation and seasonal variations of particles in the atmosphere of rural, urban and industrial areas: Organic compounds. Journal of Environmental Sciences 2016; 44: 45-56.

Chow JC, Watson JG, Lowenthal DH, Antony Chen LW, Motallebi N. PM2.5 source profiles for black and organic carbon emission inventories. Atmospheric Environment 2011; 45: 5407-5414.

Ciaparra D, Aries E, Booth M-J, Anderson DR, Almeida SM, Harrad S. Characterisation of volatile organic compounds and polycyclic aromatic hydrocarbons in the ambient air of steelworks. Atmospheric Environment 2009; 43: 2070-2079.

Crenn V, Fronval I, Petitprez D, Riffault V. Fine particles sampled at an urban background site and an industrialized coastal site in Northern France - Part 1: Seasonal variations and chemical characterization. Science of The Total Environment 2017; 578: 203-218.

Curtius J. Nucleation of atmospheric aerosol particles. Comptes Rendus Physique 2006; 7: 1027-1045.

Dai Q-L, Bi X-H, Wu J-H, Zhang Y-F, Wang J, Xu H, et al. Characterization and Source Identification of Heavy Metals in Ambient PM10 and PM2.5 in an Integrated Iron and Steel Industry Zone Compared with a Background Site. Aerosol and Air Quality Research 2015; 15: 875-887.

Dall'Osto M, Booth MJ, Smith W, Fisher R, Harrison RM. A Study of the Size Distributions and the Chemical Characterization of Airborne Particles in the Vicinity of a Large Integrated Steelworks. Aerosol Science and Technology 2008; 42: 981-991.

de Gouw J, Warneke C. Measurements of volatile organic compounds in the earths atmosphere using proton-transfer-reaction mass spectrometry. Mass Spectrometry Reviews 2007; 26: 223-257.

DeCarlo PF, Kimmel JR, Trimborn A, Northway MJ, Jayne JT, Aiken AC, et al. Field-deployable, high-resolution, time-of-flight aerosol mass spectrometer. Analytical Chemistry 2006; 78: 8281-8289.

Detournay A, Sauvage S, Locoge N, Gaudion V, Leonardis T, Fronval I, et al. Development of a sampling method for the simultaneous monitoring of straight-chain alkanes, straight-chain saturated carbonyl compounds and monoterpenes in remote areas. Journal of Environmental Monitoring 2011; 13: 983-990.

DREAL. L'industrie au regard de l'environnement en Nord - Pas-de-Calais - Les chiffres clés, 2011.

Flament P, Mattielli N, Aimoz L, Choël M, Deboudt K, Jong Jd, et al. Iron isotopic fractionation in industrial emissions and urban aerosols. Chemosphere 2008; 73: 1793-1798.

Fraser MP, Yue ZW, Tropp RJ, Kohl SD, Chow JC. Molecular composition of organic fine particulate matter in Houston, TX. Atmospheric Environment 2002; 36: 5751-5758.

Gard E, Mayer JE, Morrical BD, Dienes T, Fergenson DP, Prather KA. Real-Time Analysis of Individual Atmospheric Aerosol Particles: Design and Performance of a Portable ATOFMS. Analytical Chemistry 1997; 69: 4083-4091.

Gross DS, Atlas R, Rzeszotarski J, Turetsky E, Christensen J, Benzaid S, et al. Environmental chemistry through intelligent atmospheric data analysis. Environmental Modelling & Software 2010; 25: 760-769.

737 Healy RM, Hellebust S, Kourtchev I, Allanic A, O'Connor IP, Bell JM, et al. Source
738 apportionment of PM2.5 in Cork Harbour, Ireland using a combination of single particle mass
739 spectrometry and quantitative semi-continuous measurements. Atmospheric Chemistry and
740 Physics 2010; 10: 9593-9613.

741 Healy RM, O'Connor IP, Hellebust S, Allanic A, Sodeau JR, Wenger JC. Characterisation of
742 single particles from in-port ship emissions. Atmospheric Environment 2009; 43: 6408-6414.

743 Hleis D, Fernandez-Olmo I, Ledoux F, Kfoury A, Courcot L, Desmonts T, et al. Chemical
744 profile identification of fugitive and confined particle emissions from an integrated iron and
745 steelmaking plant. Journal of Hazardous Materials 2013; 250-251: 246-255.

746 Holmes NS. A review of particle formation events and growth in the atmosphere in the
747 various environments and discussion of mechanistic implications. Atmospheric Environment
748 2007; 41: 2183-2201.

749 Ji Z, Gan M, Fan X, Chen X, Li Q, Lv W, et al. Characteristics of PM2.5 from iron ore
750 sintering process: Influences of raw materials and controlling methods. Journal of Cleaner
751 Production 2017; 148: 12-22.

752 Katsoyiannis A, Sweetman AJ, Jones KC. PAH Molecular Diagnostic Ratios Applied to
753 Atmospheric Sources: A Critical Evaluation Using Two Decades of Source Inventory and Air
754 Concentration Data from the UK. Environmental Science & Technology 2011; 45: 8897-
755 8906.

756 Kelly FJ, Fussell JC. Air pollution and airway disease. Clinical & Experimental Allergy 2011;
757 41: 1059-1071.

758 Kfoury A, Ledoux F, Roche C, Delmaire G, Roussel G, Courcot D. PM2.5 source
759 apportionment in a French urban coastal site under steelworks emission influences using
760 constrained non-negative matrix factorization receptor model. Journal of Environmental
761 Sciences 2016; 40: 114-128.

762 Kulmala M, Vehkamaki H, Petaja T, Dal Maso M, Lauri A, Kerminen VM, et al. Formation
763 and growth rates of ultrafine atmospheric particles: a review of observations. Journal of
764 Aerosol Science 2004; 35: 143-176.

765 Landkocz Y, Ledoux F, André V, Cazier F, Genevray P, Dewaele D, et al. Fine and ultrafine
766 atmospheric particulate matter at a multi-influenced urban site: Physicochemical
767 characterization, mutagenicity and cytotoxicity. Environmental Pollution 2017; 221: 130-140.

768 Leoni C, Hovorka J, Dočekalová V, Cajthaml T, Marvanová S. Source Impact Determination
769 using Airborne and Ground Measurements of Industrial Plumes. Environmental Science &
770 Technology 2016; 50: 9881-9888.

771 Li W, Peng Y, Bai Z. Distributions and sources of n-alkanes in PM2.5 at urban, industrial and
772 coastal sites in Tianjin, China. Journal of Environmental Sciences 2010; 22: 1551-1557.

773 Lin C, Liou N, Chang P-E, Yang J-C, Sun E. Fugitive Coke Oven Gas Emission Profile by
774 Continuous Line Averaged Open-Path Fourier Transform Infrared Monitoring. Journal of the
775 Air & Waste Management Association 2007; 57: 472-479.

776 Lindinger W, Hansel A, Jordan A. On-line monitoring of volatile organic compounds at pptv
777 levels by means of proton-transfer-reaction mass spectrometry (PTR-MS) - Medical

778 applications, food control and environmental research. International Journal of Mass
779 Spectrometry 1998; 173: 191-241.

780 Marris H, Deboudt K, Augustin P, Flament P, Blond F, Fiani E, et al. Fast changes in
781 chemical composition and size distribution of fine particles during the near-field transport of
782 industrial plumes. Science of The Total Environment 2012; 427-428: 126-138.

783 Marris H, Deboudt K, Flament P, Grobéty B, Gieré R. Fe and Mn Oxidation States by TEM-
784 EELS in Fine-Particle Emissions from a Fe-Mn Alloy Making Plant. Environmental Science
785 & Technology 2013; 47: 10832-10840.

786 Mbengue S, Alleman LY, Flament P. Size-distributed metallic elements in submicronic and
787 ultrafine atmospheric particles from urban and industrial areas in northern France.
788 Atmospheric Research 2014; 135–136: 35-47.

789 Mbengue S, Alleman LY, Flament P. Bioaccessibility of trace elements in fine and ultrafine
790 atmospheric particles in an industrial environment. Environmental Geochemistry and Health
791 2015; 37: 875-889.

792 Mbengue S, Alleman LY, Flament P. Metal-bearing fine particle sources in a coastal
793 industrialized environment. Atmospheric Research 2017; 183: 202-211.

794 Oberdörster G. Pulmonary effects of inhaled ultrafine particles. International Archives of
795 Occupational and Environmental Health 2000; 74: 1-8.

796 Peng C, Zhang F, Guo Z. Separation and Recovery of Potassium Chloride from Sintering
797 Dust of Ironmaking Works. ISIJ International 2009; 49: 735-742.

798 Pope CA, Burnett RT, Turner MC, Cohen A, Krewski D, Jerrett M, et al. Lung Cancer and
799 Cardiovascular Disease Mortality Associated with Ambient Air Pollution and Cigarette
800 Smoke: Shape of the Exposure–Response Relationships. Environmental Health Perspectives
801 2011; 119: 1616-1621.

802 Riffault V, Arndt J, Marris H, Mbengue S, Setyan A, Alleman LY, et al. Fine and ultrafine
803 particles in the vicinity of industrial activities: A review. Critical Reviews in Environmental
804 Science and Technology 2015; 45: 2305-2356.

805 Roukos J, Locoge N, Sacco P, Plaisance H. Radial diffusive samplers for determination of 8-h
806 concentration of BTEX, acetone, ethanol and ozone in ambient air during a sea breeze event.
807 Atmospheric Environment 2011; 45: 755-763.

808 Roukos J, Riffault V, Locoge N, Plaisance H. VOC in an urban and industrial harbor on the
809 French North Sea coast during two contrasted meteorological situations. Environmental
810 Pollution 2009; 157: 3001-3009.

811 Sanderson P, Delgado-Saborit JM, Harrison RM. A review of chemical and physical
812 characterisation of atmospheric metallic nanoparticles. Atmospheric Environment 2014; 94:
813 353-365.

814 Santos G, Fernández-Olmo I, Irabien Á, Ledoux F, Courcot D. Estimating airborne heavy
815 metal concentrations in Dunkerque (northern France). Arabian Journal of Geosciences 2016;
816 9: 231.

Setyan A, Patrick M, Wang J. Very low emissions of airborne particulate pollutants measured from two municipal solid waste incineration plants in Switzerland. Atmospheric Environment 2017; 166: 99-109.

Setyan A, Song C, Merkel M, Knighton WB, Onasch TB, Canagaratna MR, et al. Chemistry of new particle growth in mixed urban and biogenic emissions – insights from CARES. Atmospheric Chemistry and Physics 2014; 14: 6477-6494.

Setyan A, Zhang Q, Merkel M, Knighton WB, Sun Y, Song C, et al. Characterization of submicron particles influenced by mixed biogenic and anthropogenic emissions using high-resolution aerosol mass spectrometry: results from CARES. Atmospheric Chemistry and Physics 2012; 12: 8131-8156.

Stull RB. An Introduction to Boundary Layer Meteorology: Kluwer Academic Publishers, 1988.

Taiwo AM, Harrison RM, Shi Z. A review of receptor modelling of industrially emitted particulate matter. Atmospheric Environment 2014; 97: 109-120.

Talbot C, Augustin P, Leroy C, Willart V, Delbarre H, Khomenko G. Impact of a sea breeze on the boundary-layer dynamics and the atmospheric stratification in a coastal area of the North Sea. Boundary-Layer Meteorology 2007; 125: 133-154.

Weingartner E, Saathoff H, Schnaiter M, Streit N, Bitnar B, Baltensperger U. Absorption of light by soot particles: determination of the absorption coefficient by means of aethalometers. Journal of Aerosol Science 2003; 34: 1445-1463.

Weitkamp EA, Lipsky EM, Pancras PJ, Ondov JM, Polidori A, Turpin BJ, et al. Fine particle emission profile for a large coke production facility based on highly time-resolved fence line measurements. Atmospheric Environment 2005; 39: 6719-6733.

Wong HKT, Banic CM, Robert S, Nejedly Z, Campbell JL. In-stack and in-plume characterization of particulate metals emitted from a copper smelter. Geochemistry-Exploration Environment Analysis 2006; 6: 131-137.

Wu Y, Ge X, Wang J, Shen Y, Ye Z, Ge S, et al. Responses of secondary aerosols to relative humidity and photochemical activities in an industrialized environment during late winter. Atmospheric Environment 2018; 193: 66-78.

Xiang Y, Delbarre H, Sauvage S, Léonardis T, Fourmentin M, Augustin P, et al. Development of a methodology examining the behaviours of VOCs source apportionment with micro-meteorology analysis in an urban and industrial area. Environmental Pollution 2012; 162: 15-28.

Yang Z, Tang S, Zhang Z, Liu C, Ge X. Characterization of PM10 surrounding a cement plant with integrated facilities for co-processing of hazardous wastes. Journal of Cleaner Production 2018; 186: 831-839.

Zhang R, Khalizov A, Wang L, Hu M, Xu W. Nucleation and Growth of Nanoparticles in the Atmosphere. Chemical Reviews 2012; 112: 1957-2011.

Table 1. List of selected elemental ratios for the stacks and the sampling site (data from ICP/MS and ICP/AES analyses).

		Mn/Fe	Mn/Al	Fe/Ca	Na/Mg	V/Ni	Zn/Pb	Cu/Sb	Pb/Cd
Stacks	Firing area (A)	2.62	2.99	0.91	<DL	0.34	0.07	12.2	15.0
	Cooling area (B)	3.34	3.59	4.19	<DL	0.53	0.51	70.0	21.3
	Smelting unit (C)	0.46	1.25	2.86	2.47	0.00	11.9	<DL	46.3
Sampling site	15-17/5	0.67	0.86	0.70	2.23	0.62	1.03	10.2	36.6
	17-19/5	0.26	0.34	1.07	0.43	0.19	5.56	10.4	31.3
	19-21/5	1.90	1.29	1.43	1.09	0.88	2.32	15.8	13.5
	21-23/5	0.59	0.24	0.61	1.92	1.01	2.00	3.15	35.7
	23-25/5	0.58	0.75	0.92	5.18	1.17	2.31	8.77	29.8
	25-27/5	0.30	1.51	1.86	2.17	1.08	3.19	11.1	19.5
	27-29/5	0.28	0.66	1.61	6.27	1.20	2.83	7.21	26.3
	29-31/5	0.73	0.43	0.43	0.35	1.12	1.52	3.55	37.7
	31/5-1/6	1.19	0.55	0.46	0.81	0.72	3.61	3.19	31.6
	1-3/6	0.39	1.29	1.48	3.43	0.79	3.48	13.2	42.2
	3-5/6	0.45	0.30	1.00	0.85	0.45	2.11	7.62	56.4
	5-6/6	0.96	0.07	0.34	0.00	0.05	4.74	2.61	15.7
	Average	0.69	0.69	0.99	2.06	0.77	2.89	8.06	31.4
	Std dev	0.47	0.46	0.51	1.98	0.38	1.31	4.31	11.9
	Median	0.59	0.61	0.96	1.51	0.84	2.58	8.20	31.5
	Min	0.26	0.07	0.34	0.00	0.05	1.03	2.61	13.5
	Max	1.90	1.51	1.86	6.27	1.20	5.56	15.8	56.4

DL: Detection Limit

860 **Table 2.** Summary of meteorological conditions and concentrations of particle- and gas-phase
861 data during specific plumes reaching the sampling site and identified with the LIDAR and
862 SODAR.

	Wind direction	NE-E	NW	SE
	Plumes	Steelworks Fe-Mn plant	Petrochemistry	Urban
	Date	26/05/2012	03/06/2012	07/06/2012
	Start time (UTC)	10:15 am	11:30 am	5:30 am
	End time (UTC)	10:45 am	12:00 pm	6:00 am
Weather station	Temperature [°C]	21.3	11.8	15.6
	Relative humidity [%]	55	94	87
	Solar radiation [W m^{-2}]	801	51	90
Sonic anemometer	Wind speed [m s^{-1}]	4.4	2.8	3.4
	Atmosphere	unstable	very unstable	unstable
Beta Gauge	$PM_{2.5}$ [µg m^{-3}]	65.7	N/A	4.5
SMPS	Particle number [#/cm^3]	154’847	5’809	7’446
HR-ToF-AMS	Org [µg m^{-3}]	16.8	2.4	1.3
	SO_4^{2-} [µg m^{-3}]	4.8	8.1	0.7
	NO_3^- [µg m^{-3}]	8.4	2.0	0.4
	NH_4^+ [µg m^{-3}]	5.1	3.5	0.4
	Cl^- [µg m^{-3}]	2.6	0.2	0.1
	Sum NR-PM_1 [µg m^{-3}]	37.7	16.2	2.9
Aethalometer	BC [µg m^{-3}]	1.3	0.4	1.0
ATOFMS	Na-rich [count hr^{-1}]	27	44	224
	K-rich [count hr^{-1}]	275	89	31
	EC [count hr^{-1}]	75	274	35
	OC & PAH [count hr^{-1}]	6	8	8
	Fe-rich [count hr^{-1}]	67	58	8
	Ca-rich [count hr^{-1}]	25	13	10
	Mn-rich [count hr^{-1}]	10	11	5
	Pb-rich [count hr^{-1}]	23	14	0
	V-rich [count hr^{-1}]	2	3	0
	Others [count hr^{-1}]	220	6	12
VOCs cartridges, TD-GC/MS	Biogenic VOCs [µg m^{-3}]	1.8	0.8	0.6
	Aromatics [µg m^{-3}]	9.1	5.7	1.5
	Alkanes [µg m^{-3}]	7.7	17.7	2.0
	Alkenes [µg m^{-3}]	8.7	3.2	2.5
	Oxygenated VOCs [µg m^{-3}]	11.5	6.2	3.9
Gas analyzers	CO [ppb]	4666	363	692
	NO_x [ppb]	N/A	15.7	12.8
	O_3 [ppb]	17.6	16.7	7.2
	SO_2 [ppb]	47.8	N/A	6.6

863

Figure 1. (a) Map of the industrial area near Grande-Synthe, with the locations of the sampling site, the emission chimneys of the ferromanganese alloy manufacturing plant, and other industries. (b) Enlarged map showing the location of the LIDAR, with the four directions scanned by the instrument every 15 minutes. (c) Wind rose plot for the entire campaign. Key: C chemical plant; G glass manufacturing factory; M metallurgy; P plastic manufacturing plant; PC petrochemistry; PP power plant; S steelworks.

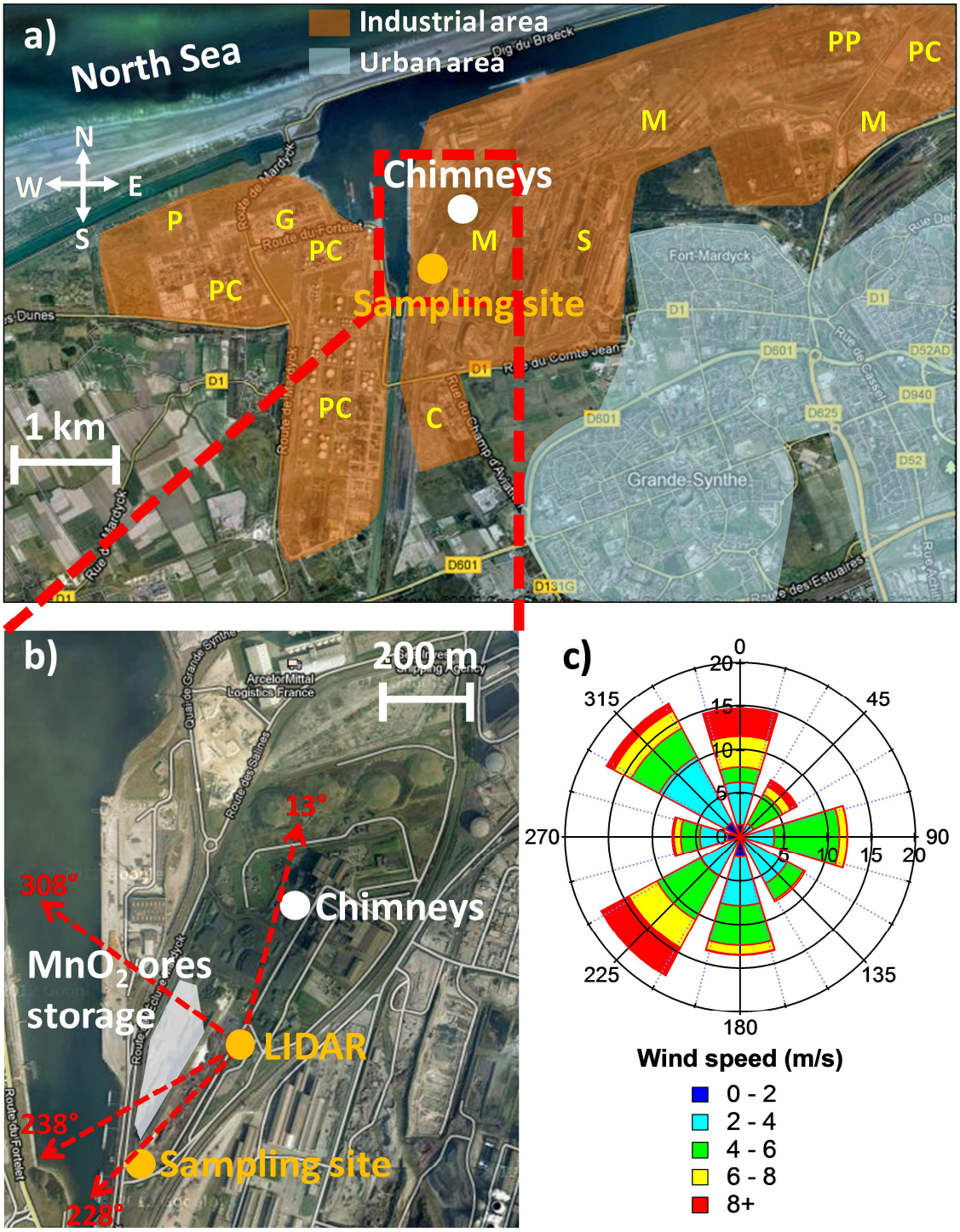

872 **Figure 2.** Schematic drawing of the ferromanganese alloy manufacturing process and the
873 filtration system used for each stack.

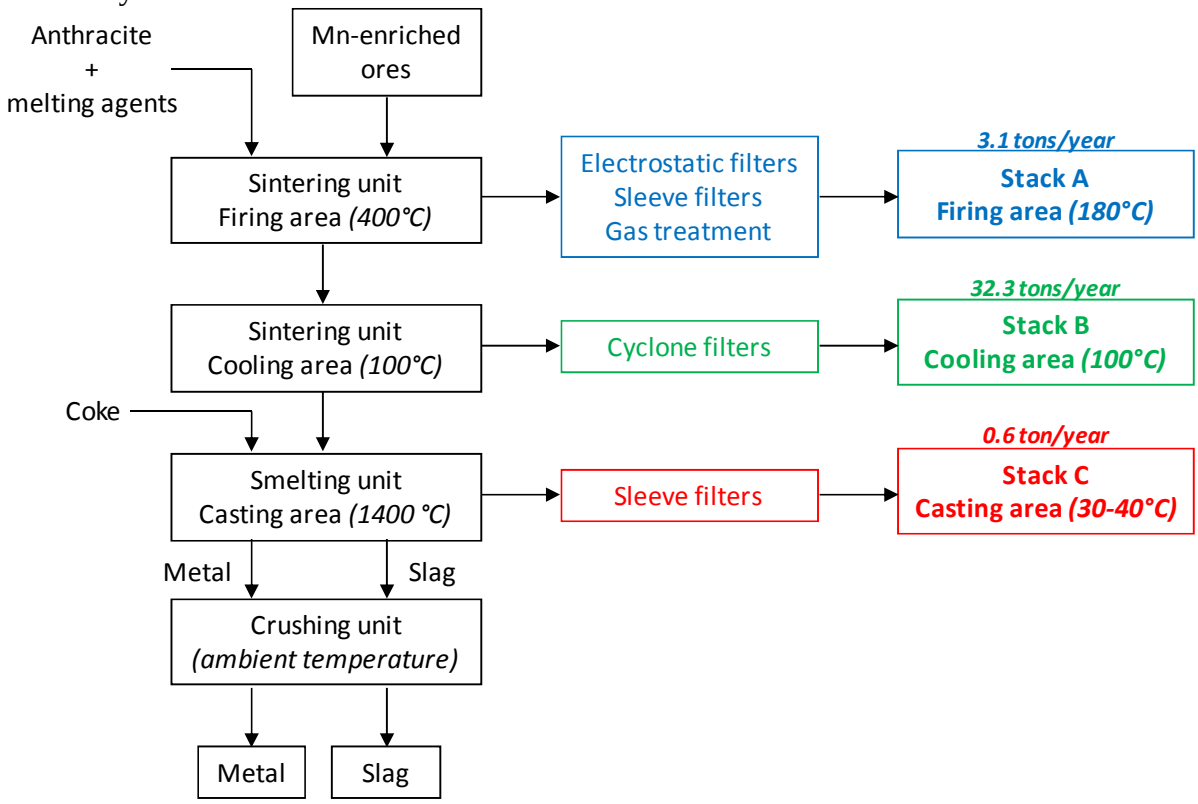

874
875

Figure 3: Time series of (a) temperature and relative humidity, (b) solar radiation and rain, (c) wind direction colored by wind speed, and (d) atmospheric stability.

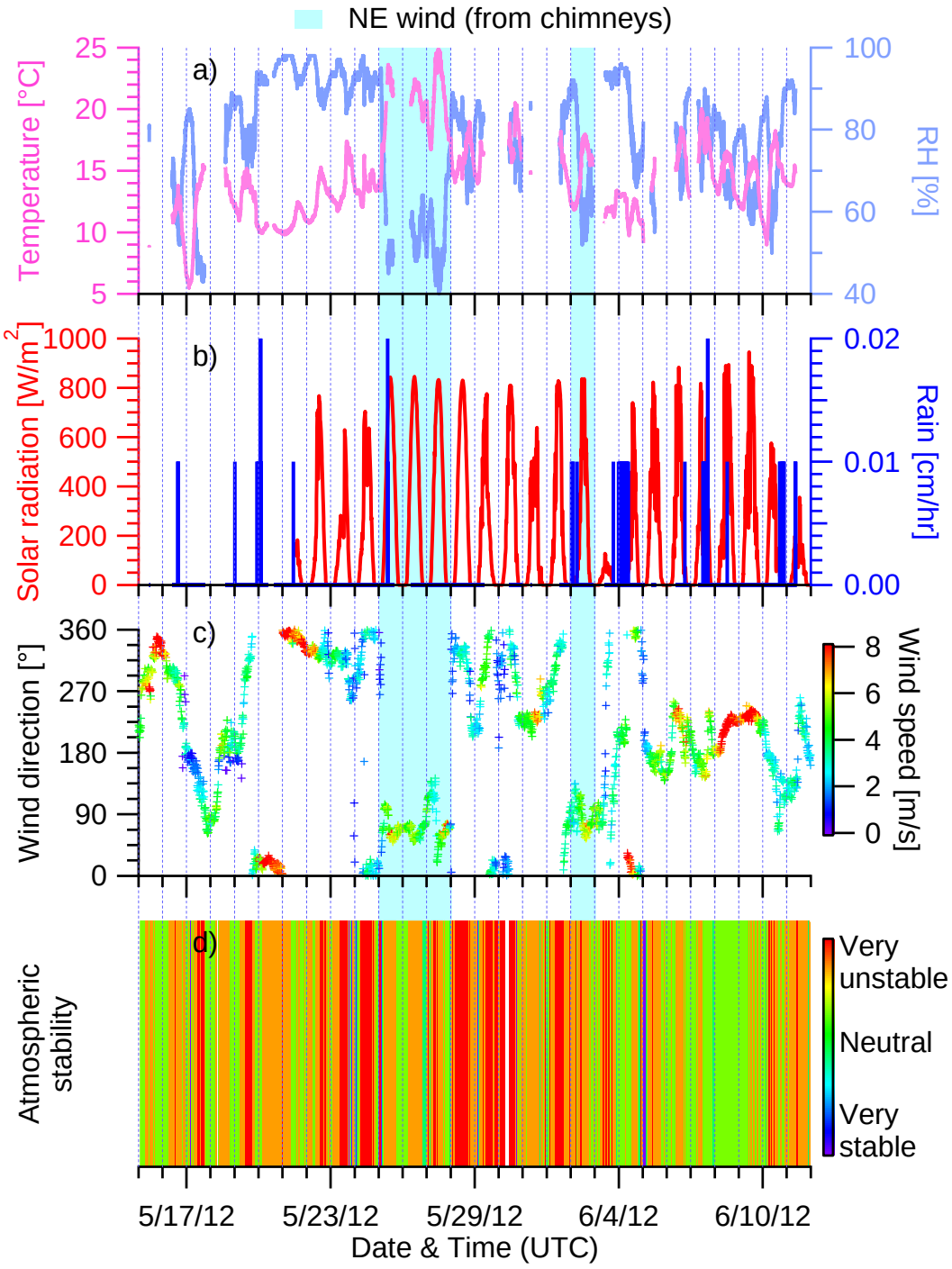

Figure 4. (a) Time-height section of wind direction and wind speed (from SODAR). (b) Time-distance section of the depolarization ratio of LIDAR at 355 nm when the instrument was pointed towards the near-field sampling site (azimuth angle 228° in Figure 1b). Time series of (c) $PM_{2.5}$ (from beta gauge), (d) particle number size distribution (from SMPS), (e) ammonium, chloride (from AMS), and BC (from Aethalometer), (f) organics, sulfate, and nitrate (from AMS) between May 25th and May 27th, 2012. The three sea breeze periods are shown on the top of the graph.

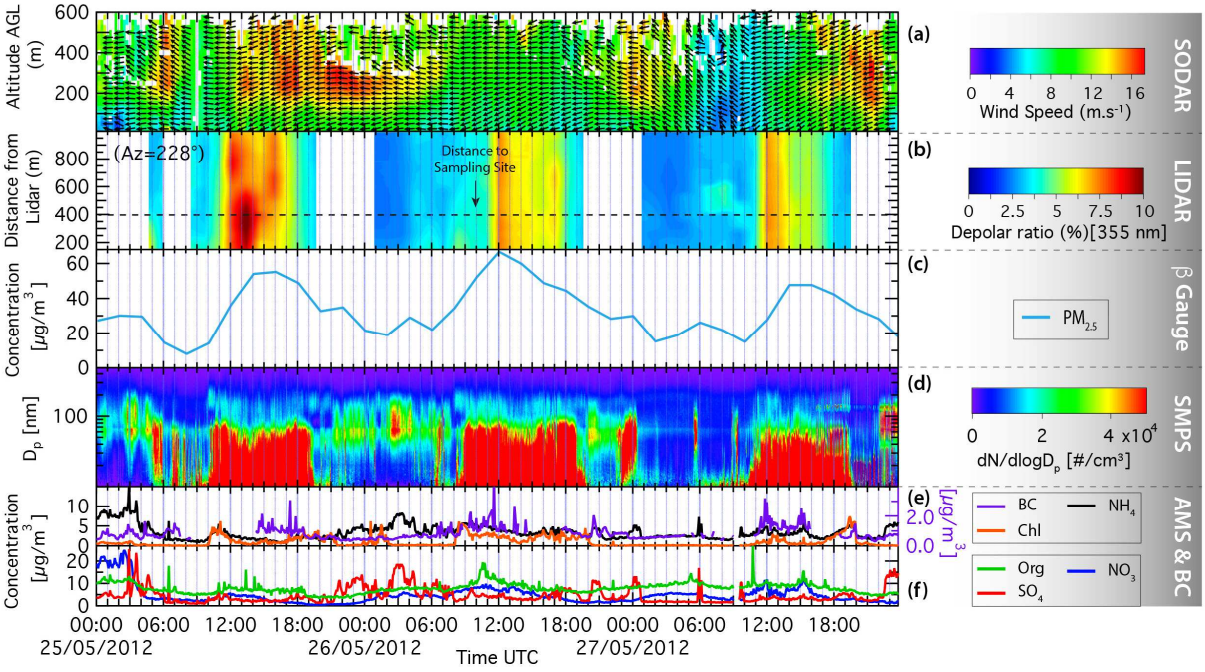

Figure 5. Time series of (a) the daily average wind direction (with length of arrows proportional to the wind speed), (b) chemical species measured by the AMS, the Aethalometer, and (c) the ATOFMS, (d) CO, CO_2, and NO_x, (e) O_3 and SO_2, (f) benzene and toluene, (g) alkanes and alkenes, (h) biogenic and oxygenated VOCs. Shaded regions correspond to NE wind periods (from stacks). The pie charts show the average contribution of the species to the total PM_1 mass and VOCs.

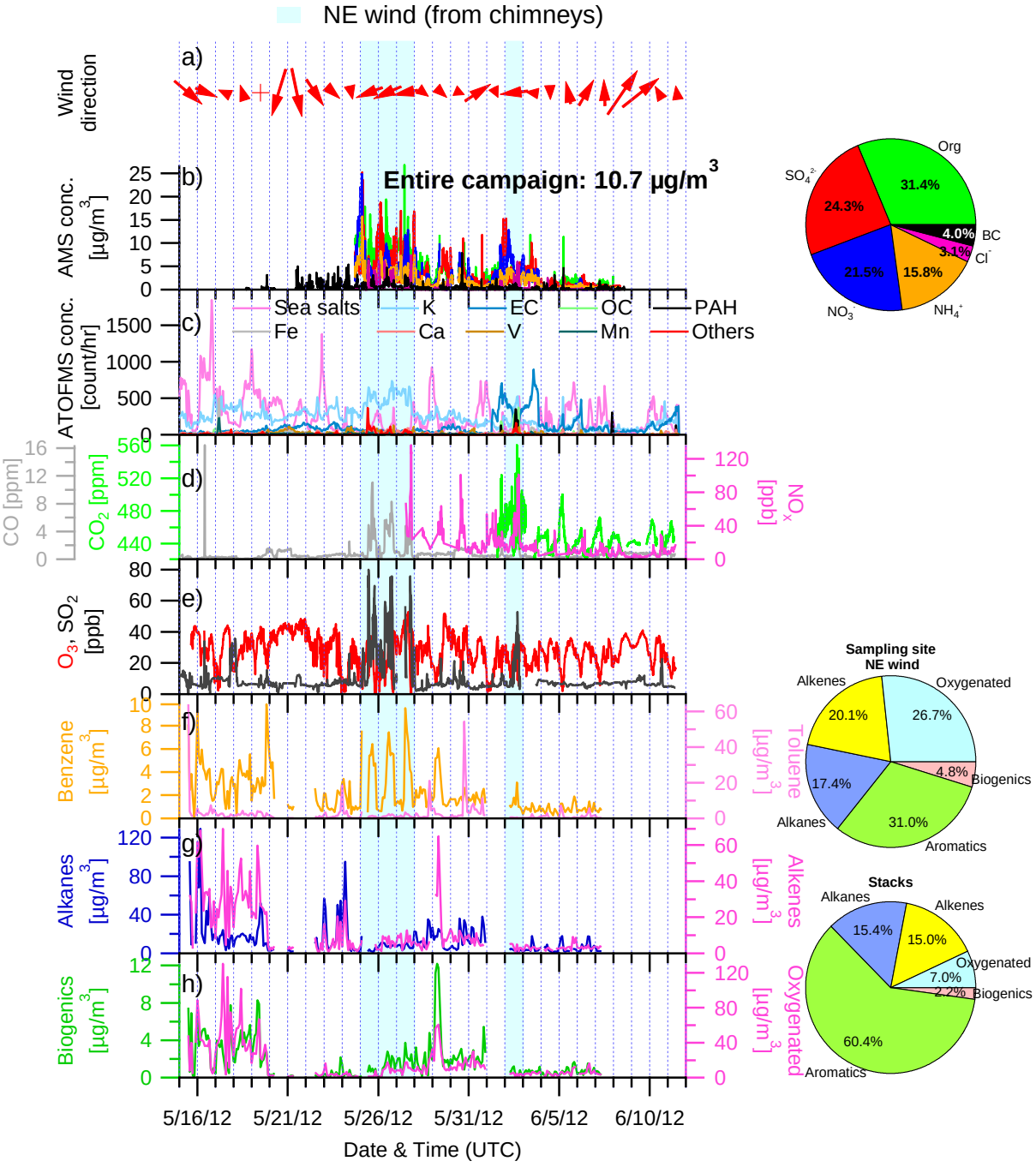

Figure 6. Time series of the size-resolved elemental composition (data from ICP/MS and ICP/AES analyses of Teflon filters), along with the average wind direction (length of arrows are proportional to wind speed).

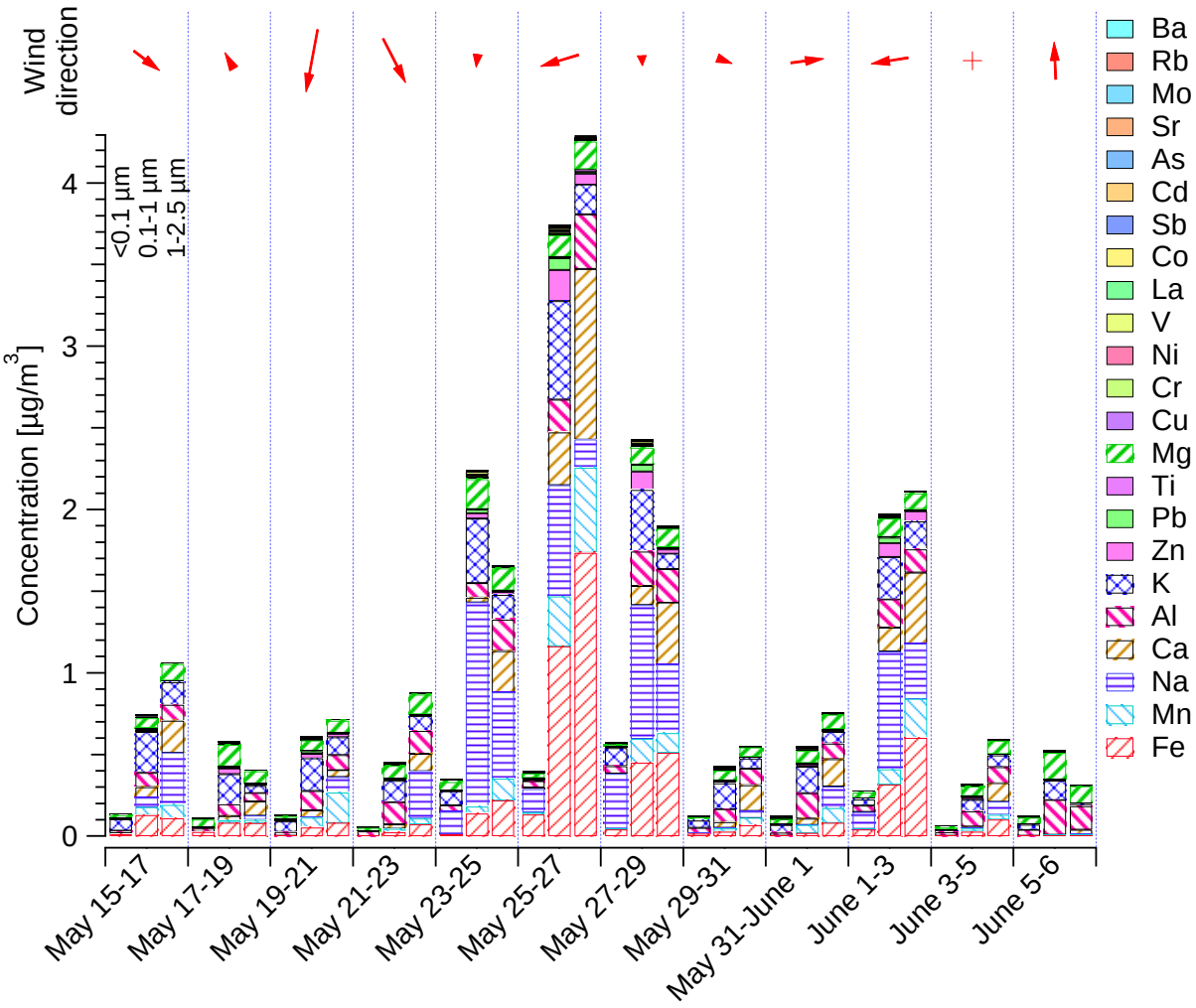

Figure 7. (a) Time series of mass size distributions at the near-field sampling site and average wind directions, and (b) average mass size distributions at the stacks of the ferromanganese alloy manufacturing plant (gravimetrically determined from 13-stage impactor filters). Sizes of arrows are proportional to the wind speed.

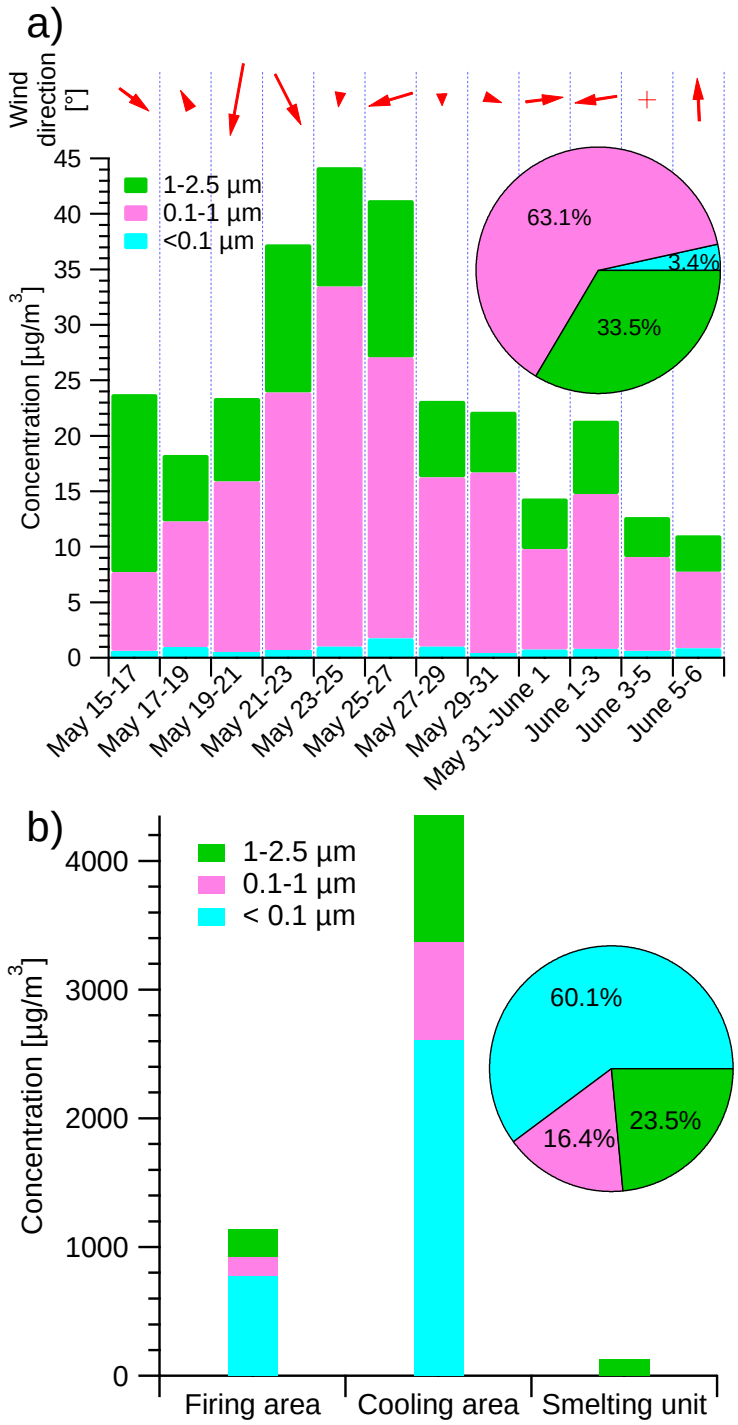

Figure 8. Time series of (a) the daily averaged wind direction (with length of arrows proportional to wind speed) and (b) the particle number size distribution. (c) Average size distributions for the entire campaign and during periods of steelworks + Fe-Mn plant, petrochemistry and urban influences (details of the periods in Table 2) (data from the SMPS).